How to cite: *Angew. Chem. Int. Ed.* **2020**, *59*, 11136–11141
International Edition: doi.org/10.1002/anie.202002693
German Edition: doi.org/10.1002/ange.202002693

Materials Science

Micro-Scale Device—An Alternative Route for Studying the Intrinsic Properties of Solid-State Materials: The Case of Semiconducting TaGeIr

*I. Antonyshyn, F. R. Wagner, M. Bobnar, O. Sichevych, U. Burkhardt, M. Schmidt, M. König, K. Poeppelmeier, A. P. Mackenzie, E. Svanidze, and Yu. Grin**

Abstract: *An efficient application of a material is only possible if we know its physical and chemical properties, which is frequently obstructed by the presence of micro- or macroscopic inclusions of secondary phases. While sometimes a sophisticated synthesis route can address this issue, often obtaining pure material is not possible. One example is TaGeIr, which has highly sample-dependent properties resulting from the presence of several impurity phases, which influence electronic transport in the material. The effect of these minority phases was avoided by manufacturing, with the help of focused-ion-beam, a μm-scale device containing only one phase—TaGeIr. This work provides evidence for intrinsic semiconducting behavior of TaGeIr and serves as an example of selective single-domain device manufacturing. This approach gives a unique access to the properties of compounds that cannot be synthesized in single-phase form, sparing costly and time-consuming synthesis efforts.*

Introduction

A comprehensive study of any new substance is only possible if we start with a high-quality material. However, it is well known that in reality crystalline materials typically contain imperfections, ranging from the macro- to the atomic-scale. Most frequently, strain, dislocations, stoichiometric deviations, and the presence of secondary phases have significant influence on physical and chemical properties, often leading to conflicting reports. Therefore, to answer some of the most pressing questions of fundamental solid-state chemistry and physics, and unlock the full application potential of solid-state materials, it is absolutely crucial to strive for the real crystal structure closest to the ideal crystallographic one. This can be achieved by growing single crystals of materials, in which it is often possible to diminish the amount of defects, that is, grain boundaries and lattice imperfections. Over the course of several decades, existing crystal-growth techniques have been significantly improved, with several new methods driven by scientific advances in condensed matter physics and solid-state chemistry.[1–4] Still, no single technique is perfect—from chemical transport[5–7] to the Bridgman method,[8,9] the Czochralski process[10–12] to the synthesis from metal fluxes[4,13–16]—all of them require a lot of optimization, which is both costly and time-consuming. The task becomes even more challenging if the necessary theoretical and/or experimental data regarding the thermodynamic properties do not exist, or the target phases are not accessible for single-crystal preparation with the techniques above. This renders the manufacturing of single-phase, let alone single-crystalline, samples nearly impossible. Naturally, the efforts become more and more laborious when the number of constituent elements is increased.

One example of such challenging material synthesis is the recently investigated compound TaGeIr, belonging to the so-called half-Heusler family. TaGeIr is one of the ABX compounds with 18 valence electrons, which were predicted[17–19] to crystallize in the cubic MgAgAs-type structure[20] (space group $F\bar{4}3m$). The crystal structure of TaGeIr, shown in the inset of Figure 1 top, may be considered as a "chameleon" atomic arrangement. From the point of view of atomic patterns, it can be viewed as the cubic closest packing of Ta (or Ge) with Ge (or Ta) and Ir in the octahedral and tetrahedral holes, respectively.[21] Alternatively, it can be understood either as the Ir–Ge or Ir–Ta zinc-blende-like network with Ta or Ge atoms on interstitial sites, respectively; or as Ta-Ge rock salt-like network with Ir atoms on interstitial sites (Wyckoff notation 4*c*) with cubic environment (heterocubane-like coordination[19,22]). Hereafter, the elemental sequence in the formulas was chosen where the first element corresponds to the one with the most positive effective charge and the third element has the most negative effective charge.[22] The stabilization of the structural pattern of MgAgAs-type is caused by the increase of ionicity (due to the charge transfer from Ta and Ge to Ir) and covalency (due to the large amount of electrons, which Ir can share with its neighbors and the appearance of covalent Ir–Ge and Ir–Ta bonds).[19] The increased ionicity and covalency of the atomic interactions are also supporting factors for appearance of the

[*] Dr. I. Antonyshyn, Dr. F. R. Wagner, Dr. M. Bobnar, Dr. O. Sichevych, Dr. U. Burkhardt, Dr. M. Schmidt, Dr. M. König, Prof. A. P. Mackenzie, Dr. E. Svanidze, Prof. Y. Grin
Max-Planck-Institut für Chemische Physik fester Stoffe
Nöthnitzer Strasse 40, 01187 Dresden (Germany)
E-mail: grin@cpfs.mpg.de
Prof. K. Poeppelmeier
Department of Chemistry, Northwestern University
2145 Sheridan Rd. Evanston, IL, 60208 (USA)
Supporting information and the ORCID identification number(s) for the author(s) of this article can be found under: https://doi.org/10.1002/anie.202002693.

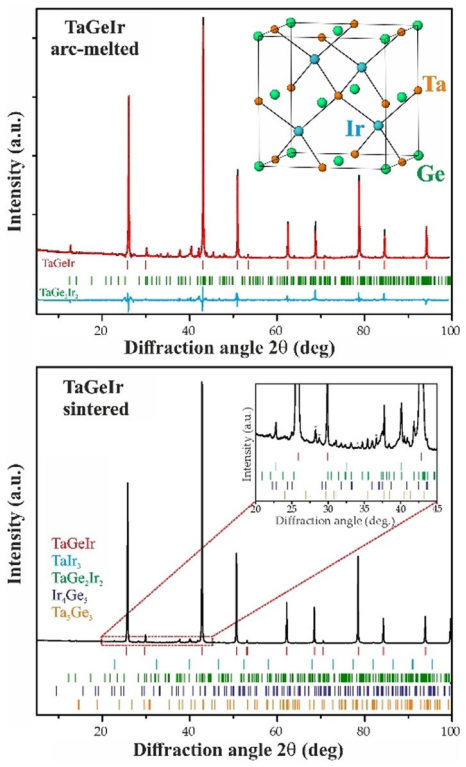

Figure 1. Powder X-ray diffraction pattern (CuK_α radiation, λ = 1.54056 Å) of the preparation products of TaGeIr by arc melting (top) and sintering (bottom). Insets: the crystal structure of TaGeIr (top) and enlarged fragment of the X-ray diffraction pattern, highlighting minority phases (asterisks) present in the sample (bottom).

band gap. The first synthesis of this substance, along with the study of its physical properties, classified this material as an indirect p-type semiconductor based on optical experiments, electronic transport properties were measured at room temperature.[23] Additional theoretical work on electronic structure and thermoelectric properties confirmed that TaGeIr should in fact be an indirect-band-gap semiconductor.[24] Further theoretical investigations suggested p-type self-doping in TaGeIr by introduction of holes via anti-site defects (Ge partially replacing Ta, for example, $Ta_{1-x}Ge_{1+x}Ir$),[25] explored pressure and charge carrier dependence of thermoelectric properties,[24] and confirmed the thermodynamic stability of TaGeIr and its crystallization with MgAgAs-type structure.[22]

While its existence was predicted based on first-principles thermodynamic calculations,[17,18] analysis of the binary phase diagrams suggests that this compound is not easy to make in single-phase form due to several neighboring phases, which form at high temperatures and cannot be removed by thermal treatments of reasonable duration. The measured indirect gap of 1.64 eV was on the upper limit of the calculated values ranging between 1.07 and 1.74 eV.[18,23,24]

No further experimental studies were carried out, which may perhaps be understood considering the synthesis challenges presented by TaGeIr. Typically, phase equilibria, which can be represented in the form of isothermal sections of phase diagrams, can be used to design a synthesis route. In the case of Ta-Ge-Ir system, no data about the phase diagram exist in the literature. The synthesis is additionally complicated by high melting temperatures of Ta and Ir. Motivated by the intriguing theoretical prediction of a semiconducting material comprised exclusively of metallic elements and limited experimental work on TaGeIr, as well as by the lack of temperature-dependent electrical resistivity data on TaGeIr, we set out to establish its transport properties.

Results and Discussion

In the current study, TaGeIr was synthesized in two ways. First, arc melting of constituent elements and consequent annealing (see Supporting Information) was carried out. Powder X-ray diffraction pattern reveals the presence of TaGeIr, as well as small quantities of $TaGe_2Ir_2$[26] (Figure 1, top). Additional minority phase—$TaIr_3$—was detected by metallographic analysis (see below). The refined lattice parameter of TaGeIr (a = 5.9651(2) Å) deviates from the published one (a_{lit} = 5.9664(5) Å[23]) by few estimated standard deviations. Electrical resistivity measurements (Figure 2, top) indicate two successive superconducting transitions at T_c = 4.4 K and T_c = 6.3 K, followed by metallic behavior at high temperature. However, the small superconducting volume fraction (inset of Figure 2, top) suggests an extrinsic origin of superconductivity.

The second synthesis route for TaGeIr was sintering of pressed powders of elements, following the procedure reported earlier[23] (see Supporting Information). The X-ray powder diffraction reveals that, in addition to TaGeIr, the sample contains $TaGe_2Ir_2$,[26] $TaIr_3$,[27,28] Ta_5Ge_3,[29,30] Ge_5Ir_4,[31,32] as well as elemental Ta (Figure 1, bottom; minority-phases reflections are marked by asterisks). It was therefore evident, that after heat treatment of the powders,[23] the reaction of the elemental Ta, Ir, and Ge is not complete and the sample is not in a thermodynamic equilibrium (see the microstructure analysis below). The respective transport properties of the sintered sample (Figure 2, bottom) indicate semiconducting behavior. A very small Meissner fraction (inset of Figure 2, bottom) reveals the presence of a superconducting impurity phase also within this sample.

Given the vastly different properties of TaGeIr samples synthesized via arc melting and sintering, we assumed several possible reasons for this discrepancy:

1) Structural variations, that is, is it possible that crystallographic positions of Ta, Ir, or Ge atoms are exchanged?
2) An off-stoichiometry of TaGeIr, that is, are different ground states a result of self-doping by mixed occupancy of crystallographic positions?[25]
3) Presence of secondary phases, that is, are the intrinsic properties of TaGeIr masked by those of the impurity phases?

To address these possibilities, the crystal structure of TaGeIr was investigated. Experimentally, it was refined employing the X-ray diffraction data on a single-crystal selected from the arc-melted sample. Striking features are displacement of the Ta atoms from the ideal position and

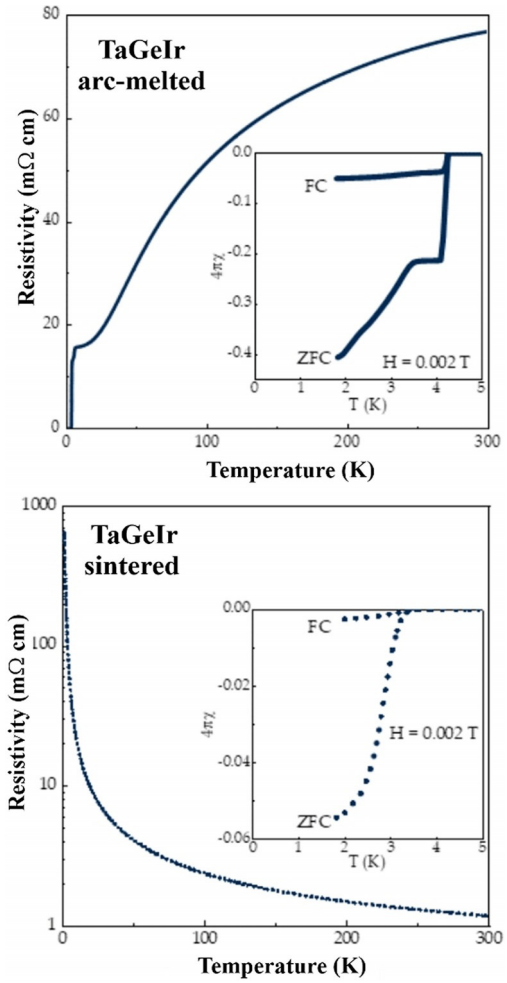

Figure 2. Magnetic and transport properties of TaGeIr samples, synthesized via arc melting (top) and sintering (bottom). The insets show Meissner fractions of the superconducting transitions (χ = magnetic susceptibility).

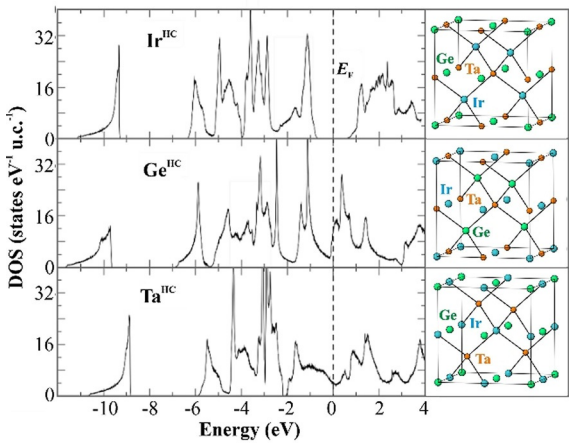

Figure 3. Electronic density of states of optimized TaGeIr models with Ir, Ge, and Ta atoms placed on the 4*c* crystallographic position, respectively (HC = heterocubane site, E_F = Fermi level). Side panels depict corresponding atomic arrangements.

mixed occupation of Ta and Ge positions. Details of the crystal structure refinement are presented in the Supporting Information (Tables S1 and S2). Furthermore, the electronic band structure was calculated for three optimized structure models (no off-center position for Ta) by placing each of three elements onto the heterocubic 4*c* site (HC in Figure 3). Note, that only the model with Ir at 4*c* (Figure 3, top) results in a band gap at the Fermi level E_F (dashed line in Figure 3), while the other two configurations yield a metal-like band structure with a non-negligible density of state at the Fermi level. In addition, the models with Ta and Ge at 4*c* site are energetically unfavorable, exhibiting an increase of energy by $+175\ kJ\ mol^{-1}$ and $+216\ kJ\ mol^{-1}$, relative to the model with Ir at 4*c*. These findings eliminate the possibility of different crystallographic arrangements in TaGeIr samples, synthesized by different means.

To examine the possibility of a non-negligible homogeneity range of TaGeIr, a series of samples with varied Ta:Ge:Ir atomic ratio was synthesized by arc melting (Figure S1). The X-ray diffraction and metallography studies indicate presence of minority phases in all synthesized samples (Tables S3 and S4), which is the reason for superconducting transitions, observed in magnetization and resistivity measurements (Figures S2 and S3). The lattice parameters of TaGeIr, summarized in Table S3, are equal within one (!) estimated standard deviation for all samples. This means that TaGeIr does not have a measurable homogeneity range, eliminating the possibility of deviations from the 1:1:1 composition, which—in turn—could change its physical properties so drastically.

Concerning the role of the minority phases, the metallographic analysis of the arc-melted TaGeIr sample clearly shows the presence of three phases, which are homogeneously distributed within the sample (Figure 4a). In addition to the main phase of TaGeIr (dark grey), two impurity phases are observed: $TaGe_2Ir_2$ (light grey) and $TaIr_3$ (white). Within the

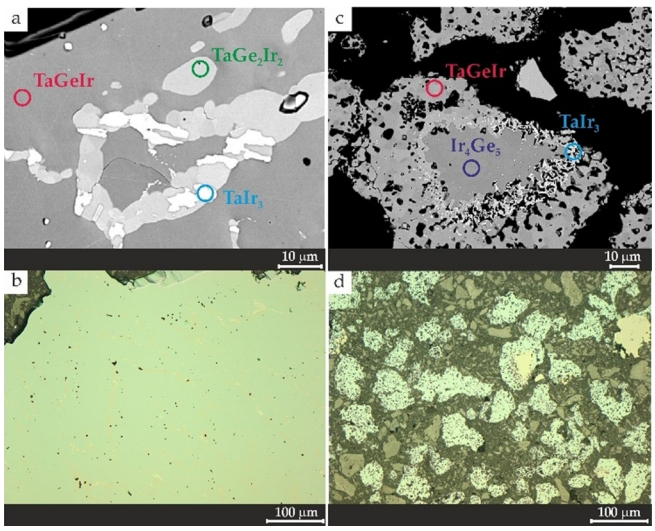

Figure 4. Microstructure of TaGeIr synthesized via arc melting (a and b) and sintering (c and d): BSE (back-scattered electrons) images (a,c) and optical bright field micrographs (b,d). The identified phases are marked on SEM images, the notation is according to Figure 1.

arc-melted sample, the distribution of $TaGe_2Ir_2$ grains provides an electrical current path, leading to metallic behavior and subsequent transition to superconductivity at $T_c = 4.4$ K. This impurity effect is further confirmed by magnetic susceptibility measurements, which indicate that less than half of the sample becomes superconducting at the lowest available temperature (inset of Figure 2, top).

On the other hand, while the sintered sample is also a multiphase one (Figures 4c,d, S4), it remains porous and inhomogeneous after the preparation procedure. The material can be considered as a μm composite one. As a consequence, no pathway for the electrical current exists, resulting in the bulk semiconducting behavior (Figure 2, bottom). The corresponding superconducting transition below 3 K involves less than 5 % of the whole sample (inset of Figure 2, bottom), which supports extrinsic origin of the superconducting transition. The presence of at least $TaGe_2Ir_2$ as an impurity was also confirmed by thermal analysis, which shows a small additional thermal effect at 1260 °C, indicating the decomposition of the 1:2:2 phase (Figure S5).

In light of these experimental constraints and driven by the search for intrinsic transport properties of TaGeIr, we have implemented micro-scale structuring in order to manufacture single-phase specimen of TaGeIr. Use of material contrast mode of the SEM (BSE regime) allowed us to identify single-phase regions of TaGeIr (blue boxes, Figures 5 top and S6) in a multi-phase polycrystalline sample (synthesis by arc-melting), which are free from sample imperfections. With this in mind, we have fabricated several micro-scale devices, with one example depicted in Figure 5 middle, using Xe-plasma focused-ion-beam patterning[33–35] (see Supporting Information for details). In a preliminary step, a slice with dimensions of around $150 \times 50 \times 2\ \mu m^3$ was cut of the bulk. Its SEM analysis reveals three phases: the main phase is TaGeIr (dark grey) and the secondary phases are $TaGe_2Ir_2$ (light grey) and $TaIr_3$ (white). Due to the small thickness of the sample, phase boundaries are visible from either side, allowing for a clear identification of single-phase regions. Therefore, the device shown in Figure 5, middle, was patterned so that the regions relevant for transport measurements include only TaGeIr (see the blue rectangles in Figures 5, top and S6). The temperature-dependent resistivity was measured in various magnetic fields. Since the data, taken on the three regions, are identical within experimental accuracy, the remainder of the discussion is focused on the results obtained on the V_1^+–V_1^- voltage pair.

As evident from Figure 5 bottom, the resistivity of TaGeIr increases monotonically as the temperature is lowered down to below 10 K, in agreement with the semiconducting behavior, predicted by band structure calculations[19,22,23] (Figure 3, top). However, the temperature dependence is relatively weak, which would not be expected for a pure semiconductor with a large band gap. At temperatures below 10 K, a decrease and subsequent sharp drop in resistivity suggest an onset of superconductivity. Owing to the high critical fields (ca. 5 T), we can rule out the possibility that this superconducting behavior is caused by the presence of the secondary phases, identified in Figure 4a, as well as other known compounds based on Ta, Ge, or Ir. Rather, the

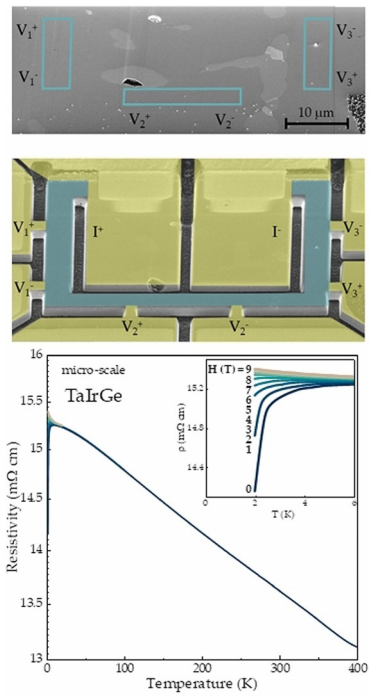

Figure 5. Application of the micro-scale device technique on polycrystalline TaGeIr sample: Top: scanning electron micrograph (BSE contrast) with TaGeIr (grey), $TaGe_2Ir_2$ (light grey), and $TaIr_3$ (white), blue rectangles mark three single-phase regions of TaGeIr selected for resistivity measurements, for the back side view cf. Figure S6; middle: micro-scale device, fabricated using focused-ion-beam patterning from the sample, shown in the top panel, yellow color represents gold contacts, while blue corresponds to the sample surface; bottom: four-terminal resistivity data, taken on the V_1^+–V_1^- voltage pair region, semiconducting behavior of TaGeIr is evident from the main panel, inset shows the low-temperature data indicating superconductivity most probably due to a thin Ta layer.

superconducting transition agrees with those of sputtered Ta films,[36] as well as other Ta-containing micro-scale structures.[37] In our case, an enrichment of Ta at the surface is unavoidable due to preferential evaporating of Ge, compared to Ir and, in particular, to Ta during the focused-ion-beam processing. So far, it has not been possible to remove the Ta layer by variation of experimental conditions. Thus, the superconducting state with $T_c \approx 2$ K and critical fields of up to 5 T should be attributed to a surface layer of Ta. Owing to the complexity of the semiconducting state in the present material, it was not possible to subtract the contribution of the tantalum film.

The observed behavior of TaGeIr is more similar to that of "non-metallic metals".[38–42] It may be understood considering either the shift of the Ta (Ge) atoms in 4*b* site from the ideal positions of the MgAgAs-type crystal structure, or the occupational disorder, or the combination of the two. Calculations of the electronic density of states in a rhombohedral model allowing the shift of the Ta (Ge) atoms from the ideal positions along the three-fold axes show that the latter—despite the atoms are shifted by approximately 0.1 Å—do not have significant influence on the electronic DOS around the Fermi level (Figure S7). Thus, the presence of Ta and/or Ge at

the heterocubic site (instead of Ir) remains as the only reason for the reduced gap, as this was suggested by the electronic DOS calculations (Figure 3). The results of the crystal structure refinement indicate that Ge appears partially at the Ta position rather than at the Ir one. The partial presence of tantalum at the iridium position is practically impossible to uniquely deduce from the crystal structure analysis. The refinement of mixed occupancies for all three positions is rather unstable to be reliable for mathematical reasons. Further DOS calculations using disordered models revealed that already with the Ta/Ir exchange of 12.5%, the new states appear in the former gap (Figure 6, top, and Figure 3, top), and the gap is going to close of the Ta/Ir exchange of 25% (Figure 6, bottom).

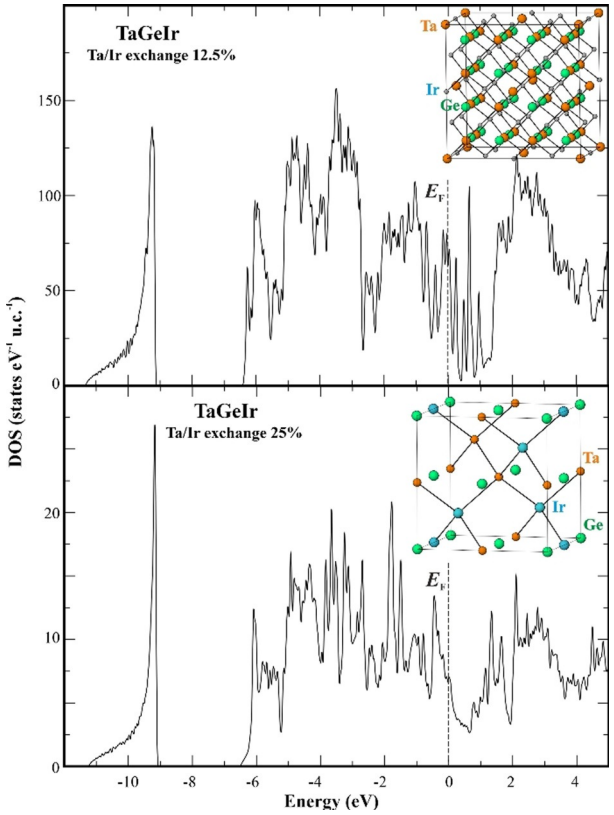

Figure 6. Electronic density of states for the disordered structural models of TaGeIr with 12.5% (top) and 25% (bottom) Ta/Ir exchange. The corresponding structural models are shown in the insets.

Conclusion

In a study of intrinsic properties of inorganic materials, particularly for intermetallic compounds, the synthesis of either single-crystal or single-phase material is the fundamental and possibly most challenging step. Frequently, the investigation of novel materials is driven by theoretical predictions, which anticipate exotic properties. Problems arise when experimental data and theoretical calculations do not agree. This was the case for TaGeIr, for which band structure calculations predict a semiconducting ground state, while resistivity data display metallic behavior with a consequent transition to superconductivity. To resolve this puzzling issue, we have manufactured a micro-scale device out of bulk TaGeIr. Upon measuring the intrinsic transport properties of TaGeIr, it was established that the material is indeed semiconducting. The modest temperature dependence can be understood by a combination of the results obtained by different techniques in a self-doping scenario, that is, strong structural disorder caused by Ta/Ir exchange producing nonmetallic-metal behavior.

This work not only conclusively identifies the ground state of an inherently challenging material, but—more generally—also provides a powerful way to study solid-state systems. The micro-scale device approach used here and in Refs. [33–35] allows the investigation of materials not accessible in single-phase form. Much like the promise of "materials by design", this technique will allow more efficient classification of materials, and much faster identification of the most promising substances. This approach may not only benefit chemists, but also physicists and material scientists, resulting in a more comprehensive and factual solid-state research.

Acknowledgements

We thank Sylvia Kostmann, Petra Scheppan and Monika Eckert for SEM experiments, Yurii Prots, Horst Borrmann and Stefan Hückmann for the help with single-crystal and powder X-ray diffraction. We are grateful to Zachary Fisk, Philip J. W. Moll, and Maja D. Bachmann for stimulating discussions. K.R.P. at Northwestern University was supported by the NSF-DMR EPM program under grant DMR-1806912.

Conflict of interest

The authors declare no conflict of interest.

Keywords: crystal structures · electronic structure · semiconductors · solid-state structures

[1] P. Gille, Yu. Grin, *Crystal Growth of Intermetallics*, De Gruyter, Berlin, **2018**.
[2] A. Prokofiev, S. Paschen, in *Modern Aspects of Bulk Crystal and Thin Film Preparation* (Eds.: N. Kolesnikov, E. Borisenko), InTech, Rijeka, **2012**, pp. 263–285.
[3] V. V. Galutskiy, M. I. Vatlina, E. V. Stroganova, *J. Cryst. Growth* **2009**, *311*, 1190.
[4] V. Yu. Verchenko, A. V. Mironov, Z. Wei, A. A. Tsirlin, E. V. Dikarev, A. V. Shevelkov, *Inorg. Chem.* **2019**, *58*, 1561.
[5] M. Binnewies, R. Glaum, M. Schmidt, P. Schmidt, *Chemical Vapor Transport Reactions*, De Gruyter, Berlin, **2012**.
[6] M. Binnewies, R. Glaum, M. Schmidt, P. Schmidt, *Z. Anorg. Allg. Chem.* **2013**, *639*, 219.
[7] P. Schmidt, M. Binnewies, R. Glaum, M. Schmidt, in *Advanced Topics on Crystal Growth* (Ed:. S. O. Ferreira), InTech, Rijeka, **2013**, pp. 8135–8326.
[8] Z. Galazka in *Handbook of Crystal Growth: Bulk Crystal Growth: Second Edition*, *Vol. 2* (Ed.: P. Rudolph), Elsevier, Amsterdam, **2015**, pp. 209–240.

[9] D. Schulz, S. Ganschow, D. Klimm, K. Struve, *J. Cryst. Growth* **2008**, *310*, 1832.
[10] G. Müller, *Cryst. Res. Technol.* **2007**, *42*, 1150.
[11] E. Talik, M. Oboz, *Acta Phys. Pol. A* **2013**, *124*, 340.
[12] E. V. Zharikov, D. A. Lis, K. A. Subbotin, V. B. Dudnikova, O. N. Zaitseva, *Acta Phys. Pol. A* **2013**, *124*, 274.
[13] D. C. Schmitt, B. L. Drake, G. T. McCandless, J. Y. Chan, *Acc. Chem. Res.* **2015**, *48*, 612.
[14] W. A. Phelan, M. C. Menard, M. J. Kangas, G. T. McCandless, B. L. Drake, J. Y. Chan, *Chem. Mater.* **2012**, *24*, 409.
[15] E. G. Moshopoulou, Z. Fisk, J. L. Sarrao, J. D. Thompson, *J. Solid State Chem.* **2001**, *158*, 25.
[16] M. G. Kanatzidis, R. Pöttgen, W. Jeitschko, *Angew. Chem. Int. Ed.* **2005**, *44*, 6996; *Angew. Chem.* **2005**, *117*, 7156.
[17] A. Zakutayev, X. Zhang, A. Nagaraja, L. Yu, S. Lany, T. O. Mason, D. S. Ginley, A. Zunger, *J. Am. Chem. Soc.* **2013**, *135*, 10048.
[18] R. Gautier, X. Zhang, L. Hu, L. Yu, Y. Lin, T. O. L. Sunde, D. Chon, K. R. Poeppelmeier, A. Zunger, *Nat. Chem.* **2015**, *7*, 308.
[19] D. Bende, F. R. Wagner, O. Sichevych, Yu. Grin, *Angew. Chem. Int. Ed.* **2017**, *56*, 1313; *Angew. Chem.* **2017**, *129*, 1333.
[20] R. Juza, F. Hund, *Naturwissenschaften* **1946**, *33*, 121.
[21] Yu. Grin, U. Schwarz, W. Steurer, in *Alloy Physics: A Comprehensive Reference* (Ed.: W. Pfeiler), Wiley-VCH, Weinheim, **2007**, pp. 19 – 62.
[22] D. Bende, F. R. Wagner, Yu. Grin, *Inorg. Chem.* **2015**, *54*, 3970.
[23] F. Yan, X. Zhang, Y. G. Yu, L. Yu, A. Nagaraja, T. O. Mason, A. Zunger, *Nat. Commun.* **2015**, *6*, 2017.
[24] J. H. Wei, G. Wang, *Appl. Phys. A* **2017**, *123*, 375.
[25] Y. G. Yu, X. Zhang, A. Zunger, *Phys. Rev. B* **2017**, *95*, 085201.
[26] L. C. Srivichitranond, E. M. Seibel, W. Xie, Z. Sobczak, T. Klimczuk, R. J. Cava, *Phys. Rev. B* **2017**, *95*, 174521.
[27] A. E. Dwight, P. A. Beck, *Trans. Am. Inst. Min. Metall. Eng.* **1959**, *215*, 976.
[28] K. I. Portnoi, V. M. Romashov, S. E. Salibekov, *Sov. Powder Metall. Met. Ceram.* **1971**, *10*, 925.
[29] H. Nowotny, A. W. Seracy, J. E. Orr, *J. Phys. Chem.* **1956**, *60*, 677.
[30] F. Yuan, S. Forbes, K. Kumar Ramachandran, Yu. Mozharivskyj, *J. Alloys Compd.* **2015**, *650*, 712.
[31] P. K. Panday, G. S. P. Singh, K. Schubert, *Z. Kristallogr.* **1967**, *125*, 274.
[32] G. Flieher, H. Völlenke, H. Nowotny, *Monatsh. Chem.* **1968**, *99*, 877.
[33] P. J. W. Moll, *Annu. Rev. Condens. Matter Phys.* **2018**, *9*, 147.
[34] F. Ronning, T. Helm, K. R. Shirer, M. D. Bachmann, L. Balicas, M. K. Chan, B. J. Ramshaw, R. D. McDonald, F. F. Balakirev, M. Jaime, E. D. Bauer, P. J. W. Moll, *Nature* **2017**, *548*, 313.
[35] A. Amon, E. Svanidze, A. Ormeci, M. König, D. Kasinathan, D. Takegami, Yu. Prots, Y.-F. Liao, K.-D. Tsuei, L. H. Tjeng, A. Leithe-Jasper, Yu. Grin, *Angew. Chem. Int. Ed.* **2019**, *58*, 15928; *Angew. Chem.* **2019**, *131*, 16075.
[36] J. J. Hauser, H. C. Theuerer, *Rev. Mod. Phys.* **1964**, *36*, 80.
[37] M. D. Bachmann, N. Nair, F. Flicker, R. Ilan, T. Meng, N. J. Ghimire, E. D. Bauer, F. Ronning, J. G. Analytis, P. J. W. Moll, *Sci. Adv.* **2017**, *3*, e1602983.
[38] A. Akrap, Y. M. Dai, W. Wu, S. R. Julian, C. C. Homes, *Phys. Rev. B* **2014**, *89*, 125115.
[39] B. M. Huddart, M. T. Birch, F. L. Pratt, S. J. Blundell, D. G. Porter, S. J. Clark, W. Wu, S. R. Julian, P. D. Hatton, T. Lancaster, *J. Phys. Condens. Matter* **2019**, *31*, 285803.
[40] S. R. Julian, C. Pfleiderer, F. M. Grosche, N. D. Mathur, G. J. McMullan, A. J. Diver, I. R. Walker, G. G. Lonzarich, *J. Phys. Condens. Matter* **1996**, *8*, 9675.
[41] A. M. Hallas, A. Z. Sharma, C. Mauws, Q. Chen, H. D. Zhou, C. Ding, Z. Gong, M. Tachibana, P. M. Sarte, J. P. Attfiled, G. M. Luke, C. R. Wiebe, *npj Quantum Mater.* **2019**, *4*, 9.
[42] E. Martino, M. D. Bachmann, L. Rossi, K. A. Modic, I. Zivkovic, H. M. Rønnow, P. J. W. Moll, A. Akrap, l. Forró, S. Katrych, *J. Phys. Condens. Matter* **2019**, *31*, 485705.

Manuscript received: February 21, 2020
Accepted manuscript online: March 22, 2020
Version of record online: April 30, 2020

